



# Fabrication and tuning of plasmonic optical nanoantennas around droplet epitaxy quantum dots by cathodoluminescence

Gilles Nogues, Quentin Merotto, Guillaume Bachelier, Eun Hye Lee, Jin Dong Song

## ► To cite this version:

Gilles Nogues, Quentin Merotto, Guillaume Bachelier, Eun Hye Lee, Jin Dong Song. Fabrication and tuning of plasmonic optical nanoantennas around droplet epitaxy quantum dots by cathodoluminescence. *Applied Physics Letters*, 2013, 102, pp.231112. 10.1063/1.4809831 . hal-00833154

HAL Id: hal-00833154

<https://hal.science/hal-00833154>

Submitted on 12 Jun 2013

**HAL** is a multi-disciplinary open access archive for the deposit and dissemination of scientific research documents, whether they are published or not. The documents may come from teaching and research institutions in France or abroad, or from public or private research centers.

L'archive ouverte pluridisciplinaire **HAL**, est destinée au dépôt et à la diffusion de documents scientifiques de niveau recherche, publiés ou non, émanant des établissements d'enseignement et de recherche français ou étrangers, des laboratoires publics ou privés.

# Fabrication and tuning of plasmonic optical nanoantennas around droplet epitaxy quantum dots by cathodoluminescence

Gilles Nogues,<sup>1, a)</sup> Quentin Merotto,<sup>1</sup> Guillaume Bachelier,<sup>2</sup> Eun Hye Lee,<sup>3</sup> and Jin Dong Song<sup>3</sup>

<sup>1)</sup> CEA/CNRS joint team “Nanophysics and Semiconductors”, Institut Néel-CNRS, BP 166, 25 rue des Martyrs, 38042 Grenoble Cedex 9, France

<sup>2)</sup> “Near-field” team, Institut Néel-CNRS, BP 166, 25 rue des Martyrs, 38042 Grenoble Cedex 9, France

<sup>3)</sup> Center for Opto-Electronic Convergence Systems, Korea Institute of Science and Technology, Seoul 136-791, Korea

(Dated: 12 June 2013)

We use cathodoluminescence to locate droplet epitaxy quantum dots with a precision  $\lesssim 50$  nm before fabricating nanoantennas in their vicinity by e-beam lithography. Cathodoluminescence is further used to evidence the effect of the antennas as a function of their length on the light emitted by the dot. Experimental results are in good agreement with numerical simulations of the structures.

PACS numbers: 42.79.-e, 78.67.-n, 42.82.-m

Keywords: nanophotonics, plasmonics, optical antennas, quantum dots, cathodoluminescence

Ever decreasing sizes and low dimensionality of semiconducting heterostructures makes it possible to operate them in the quantum regime where single photons are produced and/or detected, paving the way to applications in quantum information processing and communication. In this context a key issue of nanooptics concerns the possibility to modify and control the properties of the light coming from a single solid-state emitter (direction, polarization, temporal profile). A potential route towards this goal is to embed it in a dielectric microcavity<sup>1</sup> or a photonic waveguide<sup>2</sup>. Another promising strategy is to extend the know-how of RF electrical engineering to the optical domain by placing metallic nanostructures in the vicinity of the emitter<sup>3,4</sup>. They act as plasmonic optical nanoantennas able to enhance the emission rate of the emitter<sup>5,6</sup> and control its radiation pattern<sup>7–9</sup>. From a technological point of view, it is paramount to control both the emitter–antenna distance with a precision  $\lesssim 10$  nm, and the characteristic frequency of the plasmonic mode to tune the antenna to the emission wavelength. Precise positioning can be achieved with the help of AFM manipulation<sup>6,10</sup> or chemical functionalization<sup>8</sup>, while standard top-down fabrication techniques are better suited to define the shape of the metal nanostructure and hence its resonant frequency. In this letter, we demonstrate that cathodoluminescence (CL) combined to standard e-beam lithography is a powerful tool to achieve both goals. We use this technique to locate droplet epitaxy quantum dots (QDs) before fabricating nanoantennas of different length around them. CL is further used to characterize the effect of the antennas on the QDs’ emission properties as a function of the length.

Our target structure is shown in Fig. 1(c-d). It has already been shown to enhance the fluorescence of

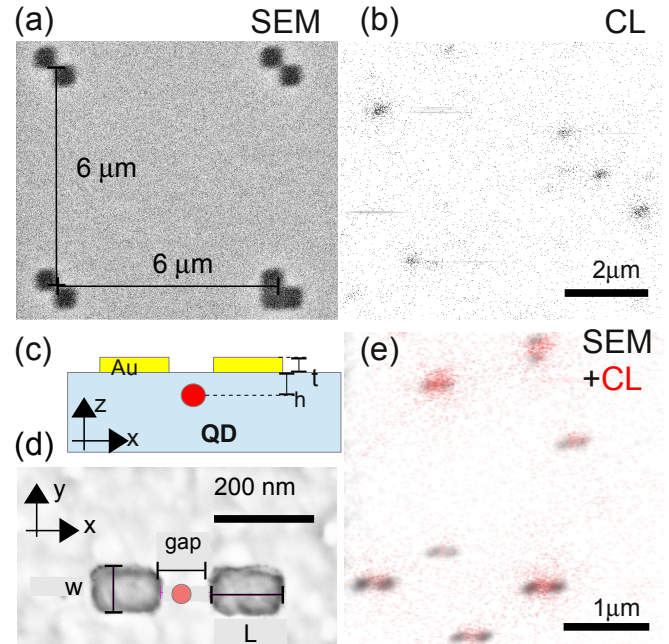


FIG. 1. Simultaneously recorded images of (a) the SEM signal of the Au alignment marks deposited on the sample and (b) the CL signal of the droplet epitaxy quantum dots ( $\lambda_{em}=750$  nm). (c) Cut and (d) top field effect SEM microphotograph of the target QD/nanoantenna assembly;  $h=50$  nm, gap 100 nm,  $w=100$  nm,  $t=35$  nm,  $L$  varies from 80 to 350 nm. (e) Composite image of the fabricated Au nanoantennas observed in SEM (black channel) and of the QD spots (red channel).

an ensemble of dye molecules<sup>11</sup>. In our case a single GaAs/AlGaAs quantum dot is buried under the gap between two Au nanostraps. QDs are produced using the modified droplet epitaxy method<sup>12</sup>. Atomic force microscopy measurements show a density of emitters of about  $3 \mu\text{m}^{-2}$ . Each dot has a typical 20 nm dia-

<sup>a)</sup> Electronic mail: gilles.nogues@grenoble.cnrs.fr

54 ter and a height of 10 nm. Capping layers of different  
 55 thickness  $h$  from 22 to 70 nm are overgrown on top of  
 56 the QD layer. Thermal annealing is necessary to activate  
 57 the luminescence of the dots<sup>13</sup>. Ensemble photoluminescence  
 58 measurements show that QDs emit between 750 and 800 nm. Microphotoluminescence and cathodo-  
 59 luminescence allow us to observe that typical signal in-  
 60 tensity from individual QD is dramatically reduced for  
 61 thicknesses  $h \leq 40$  nm. We attribute this observation to  
 62 additional nonradiative losses generated by surface in-  
 63 duced recombinations. Nanoantennas are fabricated on  
 64 a sample with  $h = 48$  nm in order to ensure the smallest  
 65 QD/antenna distance without having extra non-radiative  
 66 losses. Before localization of individual quantum dots,  
 67 Au alignment marks are fabricated onto the substrate  
 68 by e-beam lithography and sputtering of a Au layer fol-  
 69 lowed by lift-off [Fig. 1(a)]. Marks are placed on a regular  
 70 square array of period 6  $\mu\text{m}$ .

72 The sample is then observed in CL at 5 K. Light emit-  
 73 ted by the excited dots is collected by a parabolic mirror  
 74 and analyzed by a spectrometer. It is then detected by an  
 75 avalanche photodiode (APD) at the output of the spec-  
 76 trometer. A standard SEM image of the marks [Fig. 1(a)]  
 77 is simultaneously recorded with the CL image at emission  
 78 wavelength  $\lambda_{em} = 750$  nm [Fig. 1(b)]. We limit the image  
 79 acquisition time to a few seconds in order to limit the ef-  
 80 fect of thermal drift, surface contamination and charging  
 81 of the substrate in the vicinity of the quantum dot. The  
 82 presence of a QD is hence revealed by a cloud of single  
 83 photon detection counts from the APD (black pixels on  
 84 the image, typical cloud diameter  $\sim 400$  nm). The cen-  
 85 ters of the marks are determined by an edge detection  
 86 algorithm on the SEM image. The CL signal intensity  
 87 of each QD is obtained by summing all its corresponding  
 88 pixels and its position is determined by their centroid.  
 89 Combination of those informations yields the absolute  
 90 coordinates of each dot with respect to the alignment  
 91 mark array.

92 Nanoantennas are fabricated by e-beam lithography on  
 93 a 100 nm-thick PMMA layer followed by sputtering of a  
 94 35 nm thick layer of Au and lift-off. Before exposing  
 95 antennas the SEM e-beam is aligned by observing neigh-  
 96 bouring marks. For all antennas the gap between the  
 97 strips is 100 nm, the width  $w = 100$  nm and the strips  
 98 have a variable length  $L$  ranging from 80 to 360 nm.

99 After fabrication of the nanoantennas, a second CL  
 100 experiment is undertaken. Figure 1(e) presents a com-  
 101 posite image of the SEM signal (black channel) and CL  
 102 signal (red channel). It clearly shows that each an-  
 103 tenna coincides with a QD. In order to assess the perfor-  
 104 mances of our fabrication process, we have fabricated 123  
 105 QD/antenna assemblies. For each system we measure the  
 106 QD's position by its centroid as well as the antenna gap  
 107 center on the SEM image. Figure 2(a) shows a scatter  
 108 plot of the relative positions of the QDs with respect to  
 109 the nanoantennas and figure 2(b) displays an histogram  
 110 of their distance distribution. 70% of the dots are within  
 111 the 100 nm  $\times$  100 nm square defined by the gap between

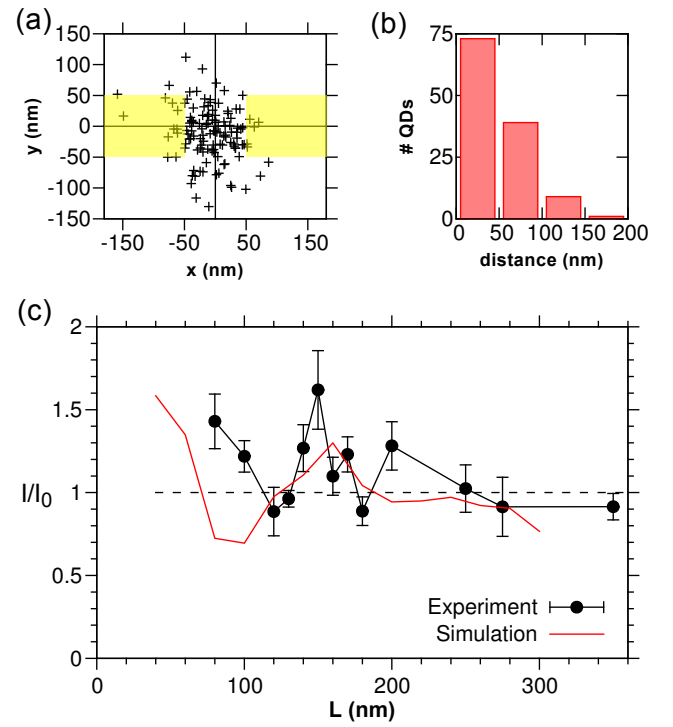


FIG. 2. (a) Scatter plot of the QD positions measured by CL with respect to the nanoantenna center. The position of the strips is shown by yellow rectangles. (b) Histogram of QDs' distance distribution from antenna center. (c) Luminescence enhancement ratio  $I/I_0$  as a function of antenna length  $L$ . Experimental points are compared to numerical simulations assuming a random distribution of dipole orientations

112 the two nanostrips. Less than 8% of them are at distances  
 113 larger than 100 nm. A qualitative study of those poorly  
 114 fabricated assemblies shows that they correspond to sys-  
 115 tems located close to the edges of the images or to other  
 116 dots. The centroid algorithm does not work properly in  
 117 those conditions. The average distance to the antenna  
 118 center is 48 nm. Assuming that it is the sum of three  
 119 independant equal sources of error (first localization, e-  
 120 beam realignment before fabrication and second local-  
 121 ization), one infers a typical localization error of 28 nm.  
 122 Our present error is larger than the target precision for  
 123 fabricating state of the art plasmonic structures, but it  
 124 is nonetheless good enough to evidence coupling of the  
 125 QD to the antenna in the case of a 100 nm gap as is our  
 126 case.

127 In order to evidence the effect of the nanoantennas  
 128 on the QDs, we compare their CL signal in presence of  
 129 the antenna  $I$  to the one measured before fabrication  $I_0$ ,  
 130 with the same parameters of beam current, dwell-time  
 131 and magnification. Hence, the excitation rate  $\gamma_{exc}$  is the  
 132 same for the two experiments. Moreover it is low enough  
 133 to ensure that the quantum dots are not saturated, i.e.  
 134  $\gamma_{exc} \ll \gamma_{tot}$  where  $\gamma_{tot}$  is the relaxation rate of the quan-  
 135 tum dot. Between 6 and 27 QD/antenna assemblies have

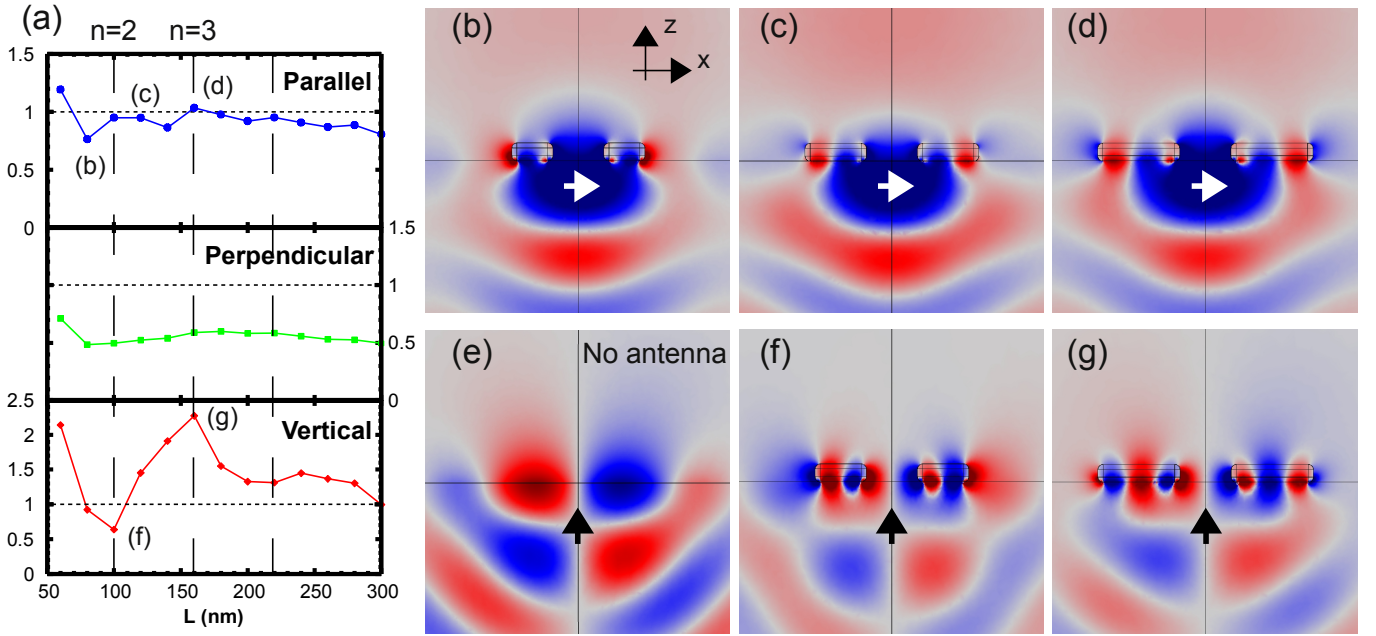


FIG. 3. (a) simulated enhancement factors as a function of antenna length  $L$  for a quantum dot corresponding to an oscillating dipole along the parallel ( $x$ ), perpendicular ( $y$ ) or vertical ( $z$ ) direction. Maps of  $\text{Re}[E_x]$  in the  $(x, z)$  plane for a parallel dipole (b-d) and a vertical dipole (f,g) for different antenna lengths. The corresponding points are shown on figure (a) except for (e).

been fabricated for each antenna length  $L$ . Figure 2(c) presents the average ratio  $I/I_0$  as a function of  $L$ . The corresponding error bars represent the statistical standard error on this value. One observes an enhancement of the signal (about 50%) below 80 nm and in the 140–170 nm range. This proves that it is possible to tune the antenna length in order to optimize the emission of light towards the CL detector. In our setup, the collection mirror is placed just above the sample and we can assume that all the light emitted on the air side of the sample is collected. The measured intensity  $I$  is then<sup>14</sup>  $I = hc/\lambda_{em} \cdot \gamma_{exc}\eta$ , where  $\eta$  is the quantum efficiency  $\eta = \gamma_{r, air}/\gamma_{tot} = \gamma_{r, air}/(\gamma_{r, air} + \gamma_{r, sub} + \gamma_{nr})$ .  $\gamma_{nr}$  is the non-radiative relaxation rate of the quantum dot. The radiative relaxation rate  $\gamma_r$  is the sum of the light emitted on the air-side and on the substrate side of the sample  $\gamma_r = \gamma_{r, air} + \gamma_{r, sub}$ .

A deeper understanding of our results arises from numerical simulations of the fabricated QD/antenna system with the finite-element software COMSOL. The QD is replaced by an electric dipole oscillating at frequency  $\nu_{em} = c/\lambda_{em}$ . We compute the power  $P_{r, air}$  (resp.  $P_{r, sub}$ ) radiated in the far-field towards the air side (resp. the substrate side) of the sample. We also evaluate the power  $P_{abs}$  absorbed in the metallic nanoantennas due to the imaginary part of the index of refraction of Au at  $\lambda_{em}$ <sup>15</sup>. As we have previously checked that surface induced nonradiative recombinations are negligible for  $h = 50$  nm, we assume that all nonradiative losses are caused by absorption, i.e.  $\gamma_{nr} \propto P_{abs}$ . We also have

$\gamma_{r, air} \propto P_{r, air}$  and  $\gamma_{r, sub} \propto P_{r, sub}$ . It is therefore possible to evaluate the quantum efficiency before and after the antenna fabrication. We perform these calculations for fixed values of  $w = 100$  nm,  $t = 35$  nm, gap = 100 nm and with various conditions of strip length  $L$  or dipole orientation. We also plot the maps of the corresponding electromagnetic fields.

The simulations show that the dipole couples to antenna modes exhibiting 1 to 3 antinodes in each nanostrip along the  $x$  axis (figure 3). From one mode to the next one,  $L$  is increased by 60 nm. This is in good agreement with half the expected surface plasmon wavelength  $\lambda_p$  for the Au/GaAs interface at frequency  $\nu_{em}$ <sup>16,17</sup>. For a dipole oriented along the  $y$  axis, the coupling to the antenna mode is poor. Hence the quantum efficiency is essentially flat and degraded to about 0.5 due to extra absorption in the metal [Fig. 3(a)]. In the case of a dipole along the  $x$  axis, the excited antenna mode radiates either in phase with the dipole, resulting in an increase of the field received by the detector [Fig. 3(b)], or in phase opposition, leading to the reverse effect [Fig. 3(c)]. The relative phase of the plasmon oscillation is shifted by  $\pi$  as  $L$  spans across the resonance condition. As a consequence the luminescence enhancement is modulated with a period  $\lambda_p/2$  with peaks at  $L = 100, 160$  and  $220$  nm. The effect of the antenna is dramatic in the case of a dipole along the  $z$  axis, which does not radiate efficiently towards the detector in absence of antenna [Fig. 3(e)]. In this configuration the dipole excites antenna modes which efficiently radiate on the air side if they have an

<sup>196</sup> odd number of antinodes [Fig. 3(g)]. For even number of  
<sup>197</sup> antinodes [Fig. 3(f)], the contributions of each antinode  
<sup>198</sup> cancel in the far field and absorption dominates. As a  
<sup>199</sup> result one observes a modulation of the emitted intensity  
<sup>200</sup> versus  $L$  with a period  $\lambda_p$ .

<sup>201</sup> As opposed to stransky-Krastanov quantum dots, the  
<sup>202</sup> orientation of the electric dipole in droplet epitaxy dots  
<sup>203</sup> is not strongly constrained due to the absence of internal  
<sup>204</sup> stress, relative large size and smooth interface. The com-  
<sup>205</sup> parison of the experimental results of figure 2(c) with the  
<sup>206</sup> simulations of figure 3(a) suggests that a large fraction of  
<sup>207</sup> systems have a dipole vertically aligned. The simulation  
<sup>208</sup> data plotted on figure 2(c) correspond to an average of  
<sup>209</sup> the three orientations. It is in good agreement with the  
<sup>210</sup> experiment.

<sup>211</sup> In summary, we have demonstrated the controlled cou-  
<sup>212</sup> pling and tuning of Au nanoantennas to droplet epitaxy  
<sup>213</sup> QDs using cathodoluminescence and standard electron-  
<sup>214</sup> beam lithography. Our method offers the advantage of  
<sup>215</sup> being spectrally selective and has a higher throughput  
<sup>216</sup> than AFM nanomanipulation techniques. The enhance-  
<sup>217</sup> ment factor of luminescence which we observe is well ex-  
<sup>218</sup> plained by numerical simulations. It could be dramati-  
<sup>219</sup> cally increased with a smaller QD/antenna distance. We  
<sup>220</sup> plan to improve the QD signal while reducing the cap-  
<sup>221</sup> ping layer. We have also developped a method for di-  
<sup>222</sup> rectly aligning the e-beam lithography setup on the CL  
<sup>223</sup> signal, thus suppressing the realignment step onto ancil-  
<sup>224</sup> lary marks<sup>18</sup>. With those two improvements, we expect  
<sup>225</sup> to fabricate coupled QD/antennas with typical depth and  
<sup>226</sup> antenna gap of the order of 20 nm. It is also possible  
<sup>227</sup> to fabricate more complicated structures like clusters of  
<sup>228</sup> nanoantennas in order to optimize the emission quantum  
<sup>229</sup> efficiency<sup>11</sup> and reach higher enhancement factors.

## <sup>230</sup> ACKNOWLEDGMENTS

<sup>231</sup> This research was supported by GRL "Development of  
<sup>232</sup> innovative photonic devices" and LIA "Center for pho-

<sup>233</sup> tonic research". The authors in KIST acknowledge the  
<sup>234</sup> support from the KIST institutional program, including  
<sup>235</sup> the Dream Project. We acknowledge the help of Institut  
<sup>236</sup> Néel's technical support teams "Nanofab" (clean room)  
<sup>237</sup> and "optical engineering" (CL setup, F. Donatini).

- <sup>238</sup> <sup>1</sup>D. Englund, D. Fattal, E. Waks, G. Solomon, B. Zhang,  
<sup>239</sup> T. Nakaoka, Y. Arakawa, Y. Yamamoto, and J. Vučković, Phys.  
<sup>240</sup> Rev. Lett. **95**, 013904 (2005).
- <sup>241</sup> <sup>2</sup>J. Claudon, J. Bleuse, N. S. Malik, M. Bazin, P. Jaffrennou,  
<sup>242</sup> N. Gregersen, C. Sauvan, P. Lalanne, and J.-M. Gérard, Nat  
<sup>243</sup> Photon **4**, 174 (2010).
- <sup>244</sup> <sup>3</sup>J.-J. Greffet, Sciences **308**, 1561 (2005).
- <sup>245</sup> <sup>4</sup>P. Mühlischlegel, H.-J. Eisler, O. J. F. Martin, B. Hecht, and  
<sup>246</sup> D. W. Pohl, Science **308**, 1607 (2005).
- <sup>247</sup> <sup>5</sup>H. Eghlidi, K. G. Lee, X.-W. Chen, S. Götzinger, and V. Sandoghdar, Nano Letters **9**, 4007 (2009), pMID: 19886647.
- <sup>248</sup> <sup>6</sup>S. Schietinger, M. Barth, T. Aichele, and O. Benson, Nano Lett. **9**, 1694 (2009).
- <sup>249</sup> <sup>7</sup>R. Esteban, T. V. Teperik, and J. J. Greffet, Phys. Rev. Lett. **104**, 026802 (2010).
- <sup>250</sup> <sup>8</sup>A. G. Curto, G. Volpe, T. H. Taminiau, M. P. Kreuzer,  
<sup>251</sup> R. Quidant, and N. F. van Hulst, Science **329**, 930 (2010).
- <sup>252</sup> <sup>9</sup>T. D. James, Z. Q. Teo, D. E. Gomez, T. J. Davis, and  
<sup>253</sup> A. Roberts, Appl. Phys. Lett. **102**, 033106 (2013).
- <sup>254</sup> <sup>10</sup>M. Pfeiffer, K. Lindfors, C. Wolpert, P. Atkinson, M. Benyoucef,  
<sup>255</sup> A. Rastelli, O. G. Schmidt, H. Giessen, and M. Lippitz, Nano  
<sup>256</sup> Letters **10**, 4555 (2010).
- <sup>257</sup> <sup>11</sup>O. L. Muskens, V. Giannini, J. A. Sánchez-Gil, and J. Gómez Rivas, Nano Letters **7**, 2871 (2007).
- <sup>258</sup> <sup>12</sup>J. Kim, B. Jo, K.-J. Lee, D. Park, C.-R. Lee, J. S. Kim, M. S.  
<sup>259</sup> Jeong, C. C. Byeon, H. Kang, J. S. Kim, J. D. Song, W. J. Choi,  
<sup>260</sup> J. I. Lee, S. J. Lee, S. K. Noh, D. K. Oh, and J.-Y. Leem, Thin  
<sup>261</sup> Solid Films **518**, 6500 (2010).
- <sup>262</sup> <sup>13</sup>P. Moon, J. D. Lee, S. K. Ha, E. H. Lee, W. J. Choi, J. D. Song,  
<sup>263</sup> J. S. Kim, and L. S. Dang, physica status solidi - (RRL) Rapid  
<sup>264</sup> Research Letters **6**, 445 (2012).
- <sup>265</sup> <sup>14</sup>P. Anger, P. Bharadwaj, and L. Novotny, Phys. Rev. Lett. **96**,  
<sup>266</sup> 113002 (2006).
- <sup>267</sup> <sup>15</sup>P. B. Johnson and R. W. Christy, Phys. Rev. B **6**, 4370 (1972).
- <sup>268</sup> <sup>16</sup>D. E. Aspnes and A. A. Studna, Phys. Rev. B **27**, 985 (1983).
- <sup>269</sup> <sup>17</sup>see Equation (2.14) from S. A. Maier, *Plasmonics: Fundamentals  
<sup>270</sup> and Applications* (Springer Science+Business Media LLC, 2007),  
<sup>271</sup> dielectric constants are taken from Refs. 15 and 16
- <sup>272</sup> <sup>18</sup>F. Donatini and L. S. Dang, Nanotechnology **21**, 375303 (2010).